Inorg. Chem. **2009**, *48*, 4010−4020

Determination of Experimental Charge Density in Model Nickel Macrocycle: [3,11-Bis(methoxycarbonyl)-1,5,9,13-tetraazacyclohexadeca-1,3,9,11-tetraenato-(2-)-κ^4N]nickel(II)

Sławomir Domagała,[†] Bohdan Korybut-Daszkiewicz,[‡] Leo Straver,[§] and Krzysztof Woźniak*,[†]

Department of Chemistry, University of Warsaw, Pasteura 1, 02-093 Warszawa, Poland, Institute of Organic Chemistry, Polish Academy of Sciences, Kasprzaka 44/52, 01-224 Warszawa, Poland, Bruker AXS, Oostsingel 209, 2612 HL Delft, The Netherlands

Received September 25, 2008

Experimental and theoretical atomic charges and d-orbital populations were obtained for [3,11-bis(methoxycarbonyl)-1,5,9,13-tetraazacyclohexadeca-1,3,9,11-tetraenato(2-)-κ^4*N*]nickel(II) monocrystal (**16Ni**) using the Hansen and Coppens formalism. Several models of this structure were tested as a function of quality of the fit, convergence of the refinement, value of residual peaks and holes, and Hirshfeld's rigid-bond test. The models with Ni-atomic scattering factors applied for the metal center are significantly better than those with the Ni-ionic scattering factors. The properties of the final electron density distributions are very consistent and similar for all of the models tested. The values of the d-orbital populations for Ni roughly agree with the occupation order of the d-electron levels for square-planar complexes derived from crystal field theory and are comparable with those obtained by the natural population analysis method. Experimental atoms-in-molecules charges calculated for four different models agree quite well for models with different symmetry restrictions and the same scattering factor for the Ni. Both experimental and theoretical methods predict relatively high negative values of charges for the nitrogen and oxygen atoms and also a quite high positive charge for the C(7) atom. The values of $\rho(\mathbf{r}_{BCP})$ for the Ni−N bonds are in the range from 0.60 up to 0.75*e* Å^{-3}, with positive laplacian values indicating noncovalent bonding. For the laplacian of the electron density evaluated in the plane of the macrocyclic ring, a typical map for a square-planar complex was obtained with four charge concentrations—3d$_{xy}$ orbitals—pointing toward the regions between the M−N bonds and charge depletions directed toward the (3,−1) critical points of the negative laplacian for the nitrogen atoms.

Introduction

According to one of the pioneers, Jean-Marie Lehn, supramolecular chemistry is a "chemistry beyond the molecule".[1,2] As conventional molecular chemistry is involved with covalent bonds, the basis of supramolecular chemistry is the noncovalent interactions, "glueing" molecules together, thus creating supramolecular species of higher complexity—supermolecules. However, this definition is not appropriate for a description of molecular machines, where the whole devices can be entirely covalently bonded molecules. In this case, the "supramolecular" term refers to all interactions between the components rather than to chemical connections.

Although, at the beginning of supramolecular chemistry, transition metals and their complexes were not regarded as useful or important components of nanoscale devices, the situation has changed. Nowadays, the transition metals are almost routinely used to build large-scale molecular structures. Such structures often exhibit interesting properties different from those of their components. Transition metals are commonly utilized to construct wires, switches, memories, logic gates, light- or electron-driven molecular motors, and 2D or 3D molecular networks.[3−18]

It is possible to design and construct devices capable of performing useful functions—molecular-level machines—by assembling specially selected molecular components. A molecular machine can be defined, by analogy to macro-

* To whom correspondence should be addressed. Tel./Fax: +48 22 8222892. E-mail: kwozniak@chem.uw.edu.pl.
[†] University of Warsaw.
[‡] Polish Academy of Sciences.
[§] Bruker AXS.

(1) Steed, J. W.; Atwood, J. L. *Supramolecular Chemistry*; Wiley: Chichester, U. K., 2000.
(2) Lehn, J.-M. *Angew. Chem., Int. Ed. Engl.* **1988**, *27*, 89–112.

10.1021/ic801835g CCC: $40.75
Published on Web 04/08/2009

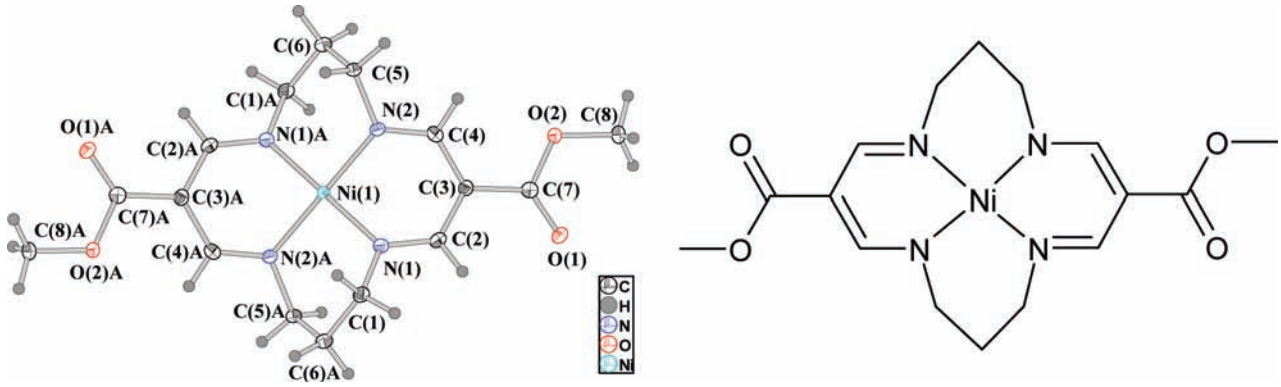

Figure 1. Thermal ellipsoids with atom numbering scheme in **16Ni**. The symmetry relation is shown using atom labels with the letter "A".

scopic devices, as an "assembly of a discrete number of structurally organised and functionally integrated molecular components designed to achieve a specific function".[3]

Previously, we reported the synthesis, electrochemical studies, and X-ray structures of a new type of homo- and hetero[2]catenanes as an example of a switchable molecular machine.[19,20] Such catenanes consist of bismacrocyclic transition-metal complexes linked by aliphatic chains and interlocked with a substituted crown ether. We have proved that, under external stimuli—electrochemical pulses—these complexes exhibit controlled intramolecular relocation of the crown ether between two positions. The relocation is possible due to $\pi\cdots\pi$ interactions between the aromatic fragments of the crown ether and the metal centers (Ni, Cu) embedded in the macrocyclic rings. The bismacrocyclic moieties were constructed from simpler tetraazamacrocyclic fragments. When two of them are linked through polymethylene chains, they form face-to-face biscyclidenes—rectangular boxlike cations.[21] These moieties can host some small guest molecules (water, π-electron-donating compounds) and are stabilized by a shell of neighboring counterions. In order to study properties of quite complex bismacrocycles and very complex catenanes, it is absolutely crucial to determine the properties of the simpler macrocyclic fragments.

We hope that this study gives us reliable quantitative numerical details of the electron density distribution of our reference system to be used jointly with similar properties of bismacrocycles and catenanes in our next projects. We would like to see the differences in the properties of electron density when two tetraazamacrocyclic systems are in such a close proximity that they do interact in the solid state. However, in order to observe consequences of such interactions, one has to use a certain reference state. By comparison to the data obtained for the monomacrocyclic system, we hope to observe significant differences in the distribution of electron density at least close to the metal centers (also, hopefully, at the other terminal fragments of the moiety). We are aiming at a quantitative analysis of such differences to prove the existence and properties of attractive interactions between atomic centers in complex supramolecular moieties which are thought by many supramolecular chemists to be only, so-called, "mechanical bonding". By use of our approach, we want to prove that such "mechanical bonds" have measurable electronic consequences.

Thus, in this work, we have focused our attention on one of our reference systems and undertaken experimental charge density studies of [3,11-bis (methoxycarbonyl)-1,5,9,13-tetraazacyclohexadeca-1,3,9,11-tetraenato(2-)-κ^4N]nickel(II) (Figure 1)—hereafter, abbreviated as **16Ni**—which is one of our reference monomacrocyclic compounds.

We have applied both experimental and theoretical methods to obtain its electronic properties. Particularly, experimental analysis of the electron density $\rho(\mathbf{r})$, based on high-resolution X-ray data, provides important information about the distribution of the electron density in molecules. We have

(3) Fabbrizzi, L.; Poggi, A. *Chemistry at the Beginning of the Third Millennium, Molecular Design, Supramolecules, Nanotechnology and Beyond*; Springer-Verlag: Berlin, 2000.
(4) Sauvage, J.-P. *Transition Metals in Supramolecular Chemistry, Perspectives in Supramolecular Chemistry*; Wiley: Chichester, 1999; Volume *5*.
(5) Dodziuk, H. *Introduction to Supramolecular Chemistry*; Kluwer: Dordrecht, The Netherlands, 2002.
(6) de Silva, A. P.; Gunaratne, H. Q. N.; Gunnlaugsson, T.; Huxley, A. J. M.; McCoy, C. P.; Rademacher, J. T.; Rice, T. E. *Chem. Rev.* **1997**, *97*, 1515–1566.
(7) Bergonzi, R.; Fabbrizzi, L.; Licchelli, M.; Mangano, C. *Coord. Chem. Rev.* **1998**, *170*, 31–46.
(8) Fabbrizzi, L.; Licchelli, M.; Pallavicini, P. *Acc. Chem. Res.* **1999**, *32*, 846–853.
(9) Amendola, V.; Fabbrizzi, L.; Licchelli, M.; Mangano, C.; Pallavicini, P.; Parodi, L.; Poggi, A. *Coord. Chem. Rev.* **1999**, *190−192*, 649–669.
(10) Hubin, T. J.; Busch, D. H. *Coord. Chem. Rev.* **2000**, *200−202*, 5–52.
(11) Collier, C. P.; Mattersteig, G.; Wong, E. W.; Luo, Y.; Beverly, K.; Sampaio, J.; Raymo, F. M.; Stoddart, J. F.; Heath, J. R. *Science* **2000**, *289*, 1172–1175.
(12) Collin, J.-P.; Dietrich-Buchecker, C. O.; Gavińa, P.; Jimenez-Molero, M. C.; Sauvage, J.-P. *Acc. Chem. Res.* **2001**, *34*, 477–487.
(13) Ballardini, R.; Balzani, V.; Credi, A.; Gandolfi, M. T.; Venturi, M. *Acc. Chem. Res.* **2001**, *34*, 445–455.
(14) Amendola, V.; Fabbrizzi, L.; Mangano, C.; Pallavicini, P. *Acc. Chem. Res.* **2001**, *34*, 488–493.
(15) Luo, Y.; Collier, C. P.; Jeppesen, J. O.; Nielsen, K. A.; Delonno, E.; Ho, G.; Perkins, J.; Hsian-Rong, T.; Yamamoto, T.; Stoddart, J. F.; Heath, J. R. *ChemPhysChem* **2002**, *3*, 519–525.
(16) Kottas, G. S.; Clarke, L. I.; Horinek, D.; Michl, J. *Chem. Rev.* **2005**, *105*, 1281–1376.
(17) Champin, B.; Mobian, P.; Sauvage, J.-P. *Chem. Soc. Rev.* **2007**, *36*, 358–366.
(18) Kay, E. R.; Leigh, D. A.; Zerbetto, F. *Angew. Chem., Int. Ed. Engl.* **2007**, *46*, 72–191.
(19) Korybut-Daszkiewicz, B.; Więckowska, A.; Bilewicz, R.; Domagała, S.; Woźniak, K. *J. Am. Chem. Soc.* **2001**, *123*, 9356–9366.
(20) Korybut-Daszkiewicz, B.; Więckowska, A.; Bilewicz, R.; Domagała, S.; Woźniak, K. *Angew. Chem., Int. Ed.* **2004**, *43*, 1668–1672.
(21) Domagała, S.; Więckowska, A.; Kowalski, J.; Rogowska, A.; Szydłowska, J.; Korybut-Daszkiewicz, B.; Bilewicz, R.; Woźniak, K. *Chem.—Eur. J.* **2006**, *12*, 2967–2981.

Table 1. Crystal Data for **16Ni**

Compound	**16Ni**
formula	$C_{16}H_{22}N_4O_4Ni$
fw	393.09
temp [K]	100
wavelength [Å]	0.71073
cryst syst	monoclinic
space group	$P2_1/c$
unit cell dimensions	
a [Å]	7.5876(5)
b [Å]	7.4404(5)
c [Å]	15.3565(11)
α [deg]	90.0
β [deg]	107.187(2)
γ [deg]	90.0
volume [Å^3]	828.23(10)
Z	2
calculated density [g cm^3]	1.576
μ [cm^{-1}]	1.20
F(000)	412
θ range for data collection	2.78−63.11
index ranges	h: −16, 18; k: −17, 18; l: −37, 37
reflns collected/unique	83634/13271
completeness to θ	93%
R_{merge}	4.81%
R_σ	2.90%
abs correction	multiscan
refinement method	full-matrix least-squares on F^2
data/restraints/params	13271/0/159
goodness-of-fit on F̂2	1.146
final R indices [$I > 2\sigma(I)$]	0.0399
R indices (all data)	0.0528
largest diff. peak and hole	0.880, −1.306

used the topological analysis of the electron density for characterization of the atomic and molecular interactions. We would like to establish quantitative details of electron density distribution in **16Ni**, topological properties of the charge density and its laplacian function, and d-orbital population.[22−24] We also want to calculate the integrated properties of atoms on the basis of experimental data using Bader's atoms-in-molecules (AIM) theory.

The experimental results are supported by quantum mechanical computational studies of the compound performed at the HF and DFT levels of theory. The above-mentioned properties will be used in subsequent papers as reference values to detect and describe the Me···Me′ interactions in bismacrocycles and—hopefully—attraction between the catenanes subunits. This is our small step toward a very great aim, which is a quantitative characterization of interactions in molecular-scale devices.

Experimental Section

Synthesis. Synthesis and structural determination of **16Ni** was already previously reported.[25]

Data Collection. Single-crystal high-resolution measurement of **16Ni** was performed using a Bruker AXS KAPPA-APEX II diffractometer up to about 0.40 Å resolution at 100 K. A single crystal of suitable size was attached to a glass fiber using silicone grease and mounted on a goniometer head in a general position. The crystal was cooled from ambient temperature to 100 K using an Oxford Instruments Cryostream. Details of the data collection procedure are given in Table 1. Data collection was done using a combination of 14 ϕ and ω runs, using a 0.5° scan width, totalling 4497 frames. The normalized scan speed ranges from 10 to 40 s/degree. Overlapping resolution areas were chosen to facilitate reliable scaling and true data multiplicity. The average multiplicity up to 0.41 Å resolution was 6.3. The short exposure scan sets were used to record the intense low-order data more accurately. Indexing, integration, and scaling were performed with original Bruker Apex software.[26] The 83 634 reflections were measured and merged to 13 271 unique reflections. The multiscan absorption correction was applied in the scaling procedure. Conventional spherical atom refinement was carried out using SHELX97[27] with the full-matrix least-squares on F^2 method for both data sets. All equivalent reflections for **16Ni** were averaged (Friedel pairs and symmetry equivalents). The lattice parameters including the final R indices obtained from spherical refinement are presented in Table 1.

Multipole Refinement. Multipole refinements of **16Ni** were accomplished using the XD program suite[28] (v. 5.02b for Windows) based on the Hansen and Coppens formalism.[29] In this formalism, the total atomic electron density is a sum of the three components:

$$\rho(\mathbf{r}) = \rho_c(r) + P_v\kappa^3\rho_v(\kappa r) + \sum_{l=0}^{l_{max}} \kappa'^3 R_l(\kappa' r) \sum_{m=0}^{l} P_{lm\pm} d_{lm\pm}(\theta, \varphi)$$

where $\rho_c(r)$ and $\rho_v(r)$ are spherical core and valence densities, respectively. The third term contains the sum of the angular functions $d_{lm\pm}(\theta,\varphi)$ to take into account aspherical deformations. The angular functions $d_{lm\pm}(\theta,\varphi)$ are real spherical harmonic functions, but normalized for the electron density. The coefficients P_v and $P_{lm\pm}$ are multipole populations for the valence and deformation density multipoles, respectively. The κ and κ' are scaling parameters introduced to make valence and deformation densities expand or contract. In the Hansen−Coppens formalism, the P_v, $P_{lm\pm}$, κ, and κ' are refineable parameters together with the atomic coordinates and thermal coefficients.

The least-squares refinement applied was based on F^2, with only those reflections with $I > 3\sigma(I)$ and with the resolution limited up to 0.45 Å to gain the data completeness around 99%. Atomic coordinates x, y, and z and anisotropic displacement parameters for each atom were taken from the spherical refinement stage and freely refined. The C−H bond distances were fixed at the averaged distances for similar groups taken from neutron data. Each atom was assigned core and spherical-valence scattering factors derived from Clementi and Roetti wave functions.[30] A single-ζ Slater-type radial function multiplied by density-normalized spherical harmonics was used for describing the valence deformation terms. The multipole expansion was truncated at the hexadecapole level for Ni. Octupole expansions for C, N, and O were applied, although the significance of the introduction of additional multipoles (hexadecapoles) was also tested (see Additional Multipoles in the Supporting Information). Only bond-oriented dipole (D0) compo-

(22) Bader, R. F. W. *Atoms in Molecules. A Quantum Theory*; Clarendon Press: Oxford, U. K., 1994.
(23) Cremer, D.; Kraka, E. *Croat. Chem. Acta* **1984**, *57*, 1259–1281.
(24) Cremer, D.; Kraka, E. *Angew. Chem., Int. Ed. Engl.* **1984**, *23*, 627–628.
(25) Rybka, A.; Koliński, R.; Kowalski, J.; Szmigielski, R.; Domagała, S.; Woźniak, K.; Więckowska, A.; Bilewicz, R.; Korybut-Daszkiewicz, B. *Eur. J. Inorg. Chem.* **2007**, 172–185.
(26) *Apex2*, v. 2.1-0; Bruker Nonius: Delft, The Netherlands, 2003, 2004; Bruker AXS: Madison, WI, 2005, 2006.
(27) Sheldrick, G. M. *SHELXL93*; University of Göttingen: Göttingen, Germany, 1993.
(28) Volkov, A.; Macchi, P.; Farrugia, L. J.; Gatti, C.; Mallinson, P.; Richter, T.; Koritsanszky, T. *XD2006*; 2006.
(29) Hansen, N. K.; Coppens, P. *Acta Crystallogr.* **1978**, *A34*, 909–921.
(30) Clementi, E.; Roetti, C. *At. Data Nucl. Data Tables* **1974**, *14*, 177.

nents for H atoms were applied. The radial fit of the valence density was optimized by refinement of the expansion−contraction parameter κ for all non-hydrogen atoms. The valence-deformation radial fits were optimized by refinement of their expansion−contraction parameters κ'. Two κ' parameters were refined for the Ni center for multipoles with $l = 2$ and $l = 4$ (the others were restricted by symmetry of the special position of the Ni atom according to the index picking rules[31]). Only one value of the κ' parameter was optimized for all $l > 0$ multipoles for all other non-hydrogen atoms of each chemical element different from Ni. During refinement, both κ and κ' for H atoms were fixed at a value of 1.20. The validity of all κ and κ' values was checked against the values obtained from multipole refinement on theoretical structure factors for a series of model compounds.[32] The 3d transition metals cause special problems when refining deformation density because of different radial extensions of the 3d and 4s valence orbitals.[33] The diffuse density corresponding to the 4s orbital contributes significantly only to a few low-angle reflections (the 4s scattering factor falls very rapidly to zero outside of this region), which is not enough to determine reliably the 4s population. Therefore, it is a common practice to fix the population of 4s density and not refine further.[34−37]

Our attempts to refine the 4s population through the $l = 0$ deformation function (second monopole) resulted in unrealistic values of the monopole populations and unstable refinement. Therefore, the models with $4s^0 3d^n$ and $4s^2 3d^n$ electron configurations of the nickel center were tested, referred to as models with Ni-ionic and -atomic scattering factors, respectively. Particular models discussed in this work are defined by the following combinations of parameters for Ni: model I, ionic scattering factor and C_i local symmetry constraint; model II, atomic scattering factor and C_i local symmetry constraint; model III, ionic scattering factor and D_{4h} local symmetry constraint; model IV, atomic scattering factor and D_{4h} local symmetry constraint. The quality of the model fit was estimated using various statistical descriptors. The equivalent values are similar in each model, although for models with Ni-atomic scattering factors of Ni the overall fit is slightly better (including statistical descriptors, residual maps). During refinement, these models converged better than the other ones. Therefore, finally only the models with Ni-atomic scattering factors (II, IV) were selected for final comparison. However, this test can not be applied alone without considering the physical meaning of the model. The adequacy of proper deconvolution of thermal motion from the bonding density for each model was tested by the Hirshfeld rigid-bond test.[38] The largest differences of mean-squares displacement amplitudes (DMSDA) values are not higher than 11×10^{-4} Å^2 for the Ni−N distances. This is only slightly larger than the upper limit expected from the test (0.0010 Å^2) and is probably due to the large difference between the nuclear masses of the bonded atoms.[39] The rest of the DMSDA values are less than 0.0010 Å^2.

The second criterion for the quality of the fit for a model is a featureless *residual density map*, $\Delta\rho^{res}(\mathbf{r}) = \rho_{obs}(\mathbf{r}) - \rho_{mul}(\mathbf{r})$, obtained from difference Fourier summation ($F_{obs} - F_{model}$). The residual map for model II is presented in Figure 1S (see the Supporting Information). The highest peaks and holes are usually located in the vicinity of the metal center. This can be caused by insufficient absorption correction for the structures containing transition metals. The residual density maps presented for **16Ni** for models I, II, III, and IV are quite flat (especially in the region farther from the metal center), with the largest residuals around the Ni atom. However, model II fits the best the experimental data (the appropriate residuals are smaller). See Table 1S in the Supporting Information for the maxima of residual peaks and holes for all models. Table 2S in the Supporting Information contains a list of the final statistical descriptors characterizing the refinement, and Table 3S in the Supporting Information gives the (*V*/*E*) ratio obtained for different models applied for **16Ni**.

AIM Integrated Atomic Charges. The atoms-in-molecules method was used for obtaining integrated atomic charges for the **16Ni** molecule. All calculations were performed using the TOPXD program, a part of the XD 4.10 package.[28] The integrated volume for each atom was divided into two parts, one of spherical shape (so-called β-sphere) and the second part defined as the shape of the atomic basin outside the β-sphere. This was done to reduce the computation cost of the integration process. Grid parameters inside and outside the β-sphere for every atom were selected on the basis of several integration tests, to give the best possible integration in a relatively small amount of time. The grid parameters inside the β-sphere were set to be the same for all atoms. All grid parameters are presented in Table 4S (Supporting Information). A check of the accuracy of the numerical integration process of the atomic properties was evaluated by calculation of the *lagrangian* function L_Ω defined as $L_\Omega = -1/4 \int_\Omega \nabla^2\rho(\mathbf{r})\, d\tau$. In favorable cases, the values of the L_Ω should be equal to 10^{-3} to 10^{-4} au (or less).[28] For the **16Ni** molecule, a rather cumbersome and demanding example, this limit could not be obtained for every atom in a reasonable amount of time. However, the sum of the integrated atoms is close to zero within an acceptable margin of error.

Computations. All ab initio calculations were performed using the Gaussian 03 program.[40] Two different quantum methods were used to calculate electronic properties of the **16Ni** molecule for comparison with the experimental charge density data. The HF with 6-31G* basis set and DFT method with (a) B3LYP 6-31G* for all atoms and (b) LAN2DZ for the metal 6-31G** basis set for all other atoms were used with full geometry optimization of the **16Ni** compound. The HF method is known to give an erroneous description of transition metal complexes, especially the M−X bond lengths, and too high Mulliken charges. The DFT methods do not

(31) Kara, M.; Kurki-Suonio, K. *Acta Crystallogr.* **1981**, *A37*, 201–210.
(32) Volkov, A.; Abramov, Y. A.; Coppens, P. *Acta Crystallogr.* **2001**, *A57*, 272–282.
(33) Coppens, P. *Coord. Chem. Rev.* **1985**, *65*, 285.
(34) Leung, P. C.; Coppens, P. *Acta Crystallogr.* **1983**, *B39*, 535–542.
(35) Farrugia, L. J.; Mallinson, P. R.; Stewart, B. *Acta Crystallogr.* **2003**, *B59*, 234–247.
(36) Stevens, E. D.; DeLucia, M. L.; Coppens, P. *Inorg. Chem.* **1980**, *19*, 813–820.
(37) Martin, M.; Rees, B.; Mitschler, A. *Acta Crystallogr.* **1982**, *B38*, 6–15.
(38) Hirshfeld, F. L. *Acta Crystallogr.* **1976**, *A32*, 239–244.
(39) Smith, G. T.; Mallinson, P. R.; Frampton, C. S.; Farrugia, L. J.; Peacock, R. D.; Howard, J. A. K. *J. Am. Chem. Soc.* **1997**, *119*, 5028–5034.
(40) Frisch, M. J.; Trucks, G. W.; Schlegel, H. B.; Scuseria, G. E.; Robb, M. A.; Cheeseman, J. R.; Montgomery, J. A., Jr.; Vreven, T.; Kudin, K. N.; Burant, J. C.; Millam, J. M.; Iyengar, S. S.; Tomasi, J.; Barone, V.; Mennucci, B.; Cossi, M.; Scalmani, G.; Rega, N.; Petersson, G. A.; Nakatsuji, H.; Hada, M.; Ehara, M.; Toyota, K.; Fukuda, R.; Hasegawa, J.; Ishida, M.; Nakajima, T.; Honda, Y.; Kitao, O.; Nakai, H.; Klene, M.; Li, X.; Knox, J. E.; Hratchian, H. P.; Cross, J. B.; Adamo, C.; Jaramillo, J.; Gomperts, R.; Stratmann, R. E.; Yazyev, O.; Austin, A. J.; Cammi, R.; Pomelli, C.; Ochterski, J. W.; Ayala, P. Y.; Morokuma, K.; Voth, G. A.; Salvador, P.; Dannenberg, J. J.; Zakrzewski, V. G.; Dapprich, S.; Daniels, A. D.; Strain, M. C.; Farkas, O.; Malick, D. K.; Rabuck, A. D.; Raghavachari, K.; Foresman, J. B.; Ortiz, J. V.; Cui, Q.; Baboul, A. G.; Clifford, S.; Cioslowski, J.; Stefanov, B. B.; Liu, G.; Liashenko, A.; Piskorz, P.; Komaromi, I.; Martin, R. L.; Fox, D. J.; Keith, T.; Al-Laham, M. A.; Peng, C. Y.; Nanayakkara, A.; Challacombe, M.; Gill, P. M. W.; Johnson, B.; Chen, W.; Wong, M. W.; Gonzalez, C.; Pople, J. A. *Gaussian 03*, Revision B.01; Gaussian, Inc.: Pittsburgh PA, 2003.

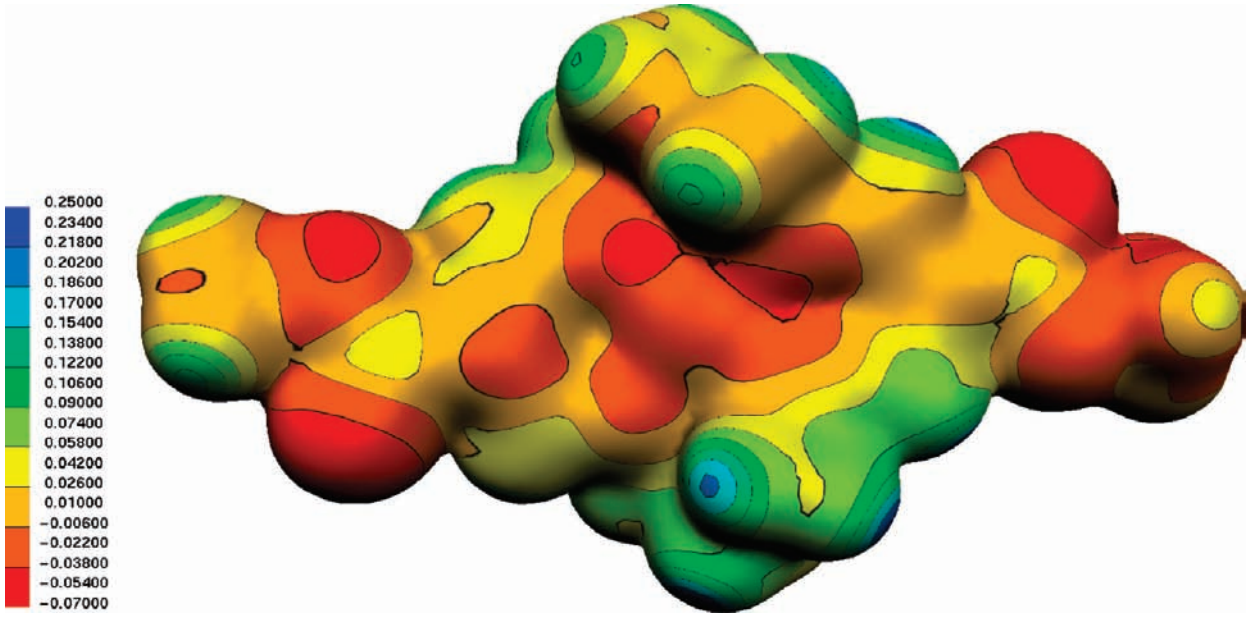

Figure 2. Envelope of electron density with the electrostatic potential mapped as generated for model II. The value of the isosurface of $\rho(\mathbf{r})$ is equal to 0.01e Å^{-3}.

Table 2. Selected Values of $\rho(\mathbf{r}_{BCP})$ and $\nabla^2\rho(\mathbf{r}_{BCP})$ (Asymmetric Part Only) at Bond Critical Points (BCPs)for **16Ni**[a]

model	II		IV	
bond	$\rho(\mathbf{r}_{BCP})$ [e Å^{-3}]	$\nabla^2\rho(\mathbf{r}_{BCP})$ [e Å^{-5}]	$\rho(\mathbf{r}_{BCP})$ [e Å^{-3}]	$\nabla^2\rho(\mathbf{r}_{BCP})$ [e Å^{-5}]
Ni(1)−N(1)	0.701(6)	11.634(6)	0.730(6)	10.936(6)
Ni(1)−N(2)	0.745(7)	11.687(7)	0.750(7)	11.306(7)
O(1)−C(7)	2.92(4)	−35.6(2)	2.92(4)	−35.7(2)
O(2)−C(7)	2.06(3)	−17.2(1)	2.06(3)	−17.1(1)
O(2)−C(8)	1.68(3)	−7.00(9)	1.68(3)	−6.87(9)
N(1)−C(1)	1.74(2)	−8.06(6)	1.74(2)	−8.06(6)
N(1)−C(2)	2.54(3)	−26.4(1)	2.54(3)	−26.3(1)
N(2)−C(4)	2.44(3)	−25.0(1)	2.44(3)	−24.9(1)
N(2)−C(5)	1.68(2)	−8.64(7)	1.69(2)	−8.67(7)
C(1)−C(6)A	1.59(3)	−8.04(5)	1.59(3)	−8.04(5)
C(2)−C(3)	2.07(3)	−16.15(7)	2.07(3)	−16.04(7)
C(3)−C(4)	1.96(3)	−14.68(6)	1.96(3)	−14.86(6)
C(3)−C(7)	1.96(3)	−14.61(6)	1.96(3)	−14.59(6)
C(5)−C(6)	1.73(3)	−11.03(5)	1.73(3)	−10.98(5)

[a] "A" denotes the 1 − X, 1 − Y, 1 − Z operation of symmetry.

possess that disadvantage and also have similar computation time requirements. The M−N bonds in the HF method are unreliably long (calculated to be 1.95 Å compared to experimental values around 1.89 Å for **16Ni**), and all Mulliken charges are larger than the corresponding values calculated by the DFT method. For all of the other parameters, bonds, valence angles, and torsional angles, the values are very similar to the experimental ones. Because of a questionable reliability of the Mulliken population analysis, the natural population analysis (NPA)[41] was also used. This method provides electronic state populations for atomic shells, which can be directly compared with orbital populations obtained from the multipole refinement.

Results and Discussion

Structure. The **16Ni** molecules crystallize in the $P2_1/c$ space group at a special position—the inversion center. Therefore, only half of the molecule is independent. The Ni atom is in a square-planar environment coordinated by four nitrogen atoms. The whole molecule deviates from the planar conformation because of the strain caused by two propylene bridges. The molecule is substituted by two methoxycarbonyl groups at the meso positions. The **16Ni** molecule with atom labels is presented in Figure 1. The envelope of the electron density is shown in Figure 2.

Topological Analysis. It appears that different models (I, II, III, and IV) are fitted almost equally well to the experimental data (see Table 2). The greatest differences in $\rho(\mathbf{r}_{BCP})$ and $\nabla^2\rho(\mathbf{r}_{BCP})$ values are obtained for the Ni−N bonds. However, the most reasonable values (with the smallest standard deviations and the deviations from the mean values) of $\rho(\mathbf{r}_{BCP})$ and $\nabla^2\rho(\mathbf{r}_{BCP})$ at the chemically equivalent bonds are obtained for the models with the Ni-atomic scattering factors (models II and IV). The second derivative of the electron density at the critical points, $\nabla^2\rho(\mathbf{r}_{BCP})$, is more sensitive to subtle changes of the model parameters. Therefore, its value is less reproducible within different models.

The topological properties of covalent bonds involving transition metals do not have the same characteristics as

(41) Reed, A. E.; Weinstock, R. B.; Weinhold, F. *J. Chem. Phys.* **1985**, *83*, 735–746.

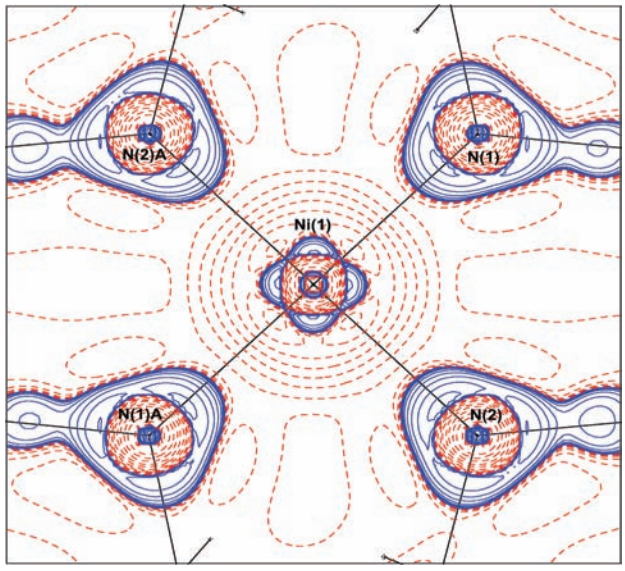

Figure 3. Negative laplacian maps in the plane defined by the metal ion center and four nitrogen atoms in **16Ni** (model II). The blue solid lines and red dashed lines indicate positive and negative values of the L(**r**), respectively. The contour spacing is in steps of $0.05 \times 2^{n-1}$ (positive values) and $-0.05 \times 2^{n-1}$ (negative values) in e Å^{-5} for $n = 1-50$. The letter "A" in the labels of atoms denotes the $1 - X$, $1 - Y$, $1 - Z$ operation of symmetry.

covalent bonds between the first-row atoms. The $\rho(\mathbf{r}_{BCP}) < 1$ values for the M−N bonds, the positive $\nabla^2\rho(\mathbf{r}_{BCP})$, and small negative values of $H(\mathbf{r}_{BCP})$ indicate shared-type interactions between the metal and ligand, typical for the transition metal complexes.[35,42−44] Values of $\rho(\mathbf{r}_{BCP}) > 1$ and a negative laplacian function of the electron density for all of the other bonds are observed for covalently bonded atoms. The kinetic energy densities at the bond critical point (BCPs), $G(\mathbf{r}_{BCP})$, given in Table 5S (Supporting Information), were estimated using the functional approximation of Abramov,[45] while the corresponding potential energy densities at the BCPs, $V(\mathbf{r}_{BCP})$, were obtained from the local virial relationship, as shown by Bader.[22] All of these values are in good agreement with the results published for similar systems.[46,47] Especially, there is good agreement between values of $\rho(\mathbf{r}_{BCP})$ and $\nabla^2\rho(\mathbf{r}_{BCP})$ compared to those of the other similar square-planar Ni complexes.[48,49] However, the values of $\rho(\mathbf{r})$ and $\nabla^2\rho(\mathbf{r})$ at the M−N BCP are smaller for our complex, which corresponds to the longer bond (1.891 Å compared to 1.928 Å).

The valence shell charge concentration (VSCC) around the Ni center is presented via negative laplacian of the density function, $L(\mathbf{r}) \equiv -\nabla^2\rho(\mathbf{r})$, in Figure 3. The $L(\mathbf{r})$ value is negative for BCPs on the M−N bonds. The VSCCs of the Ni and nitrogen atoms are not in direct contact. This is rather a typical situation for interactions other than covalent ones in transition metal complexes.[48,50,51] The shells around the N atoms, coordinating the Ni center, exhibit three charge concentrations (CCs). These are (+3,−3) CPs of $L(\mathbf{r})$, arranged around nitrogen in the shape of a triangle. One of charge concentration is pointing toward the charge depletion of the Ni atom; the other ones are directed toward the nearest bonded carbon atoms. There are four CCs around Ni in the plane of the four nitrogen atoms (Figure 3) pointing to the regions between the M−N bonds. The maxima of charge concentrations for the metal atom occur in the third electron shell and, thus, are identified with the density of the 3d orbitals.[52] The X and Y axes of the local coordinate system around Ni(1) point to nitrogen atoms, while the Z axis is perpendicular to the XY plane. Thus, these four CCs can be associated with the $3d_{xy}$ orbitals.

Atomic graphs show the topology of the laplacian of electron density. The critical points of $L(\mathbf{r})$ create a polyhedron, vertices (V), edges (E), and faces (F) which are (+3,−3), (+3,−1) and (+3,+1) CPs, respectively. The vertices denote the maxima in charge concentration, while faces denote the charge depletion regions in VSCC. Such a graph is classified by its characteristic set numbers indicating CPs, $[V,E,F]$ satisfying Euler's formula $V - E + F = 2$ for polyhedra. According to Euler's formula: for any convex polyhedron, the number of vertices and faces together is exactly two more than the number of edges. For instance, a tetrahedron has four vertices, four faces, and six edges; thus, $4 - 6 + 4 = 2$. A characteristic arrangement of the CPs of $L(\mathbf{r})$ depends on the coordination of the transition metal atom. Polyhedra shapes for different coordinations such as tetragonal, octahedral, or spherical have already been reported in numerous articles.[47,51,53,54] However, the atomic graphs presented in Figure 4 for the Ni atom of the **16Ni** molecule are completely different. Unlike systems with octahedral, tetragonal, or spherical coordination, the **16Ni** complex is a square-planar system, which influences the topology of the laplacian around the Ni atom. The graph is no longer a polyhedron, but a planar graph with (+3,−3) CCs located at the corners of the square, each joined with four nearest (+3,−1) CPs. The (+3,+1) charge depletion regions are located along the M−N bonds, also above and below the plane defined by the nitrogen and nickel atoms. The atomic graph can be classified as the [4,8,6] form, still satisfying Euler's formula. The square-planar coordination can be derived from the octahedral arrangement by pulling out two of the ligands along the Z axis to infinity. Therefore, the atomic graph for the square-planar complexes should be a distinct form obtained from the octahedral graph. Indeed, by bringing the (+3,−3) critical points of a typical octahedral

(42) Macchi, P.; Proserpio, D. M.; Sironi, A. *J. Am. Chem. Soc.* **1998**, *120*, 1447–1455.
(43) Macchi, P.; Proserpio, D. M.; Sironi, A. *J. Am. Chem. Soc.* **1998**, *120*, 13429–13435.
(44) Macchi, P.; Garlaschelli, L.; Martinego, S.; Sironi, A. *J. Am. Chem. Soc.* **1999**, *121*, 10428–10429.
(45) Abramov, Y. A. *Acta Crystallogr.* **1997**, *A53*, 264–272.
(46) Kožíšek, J.; Hansen, N. K.; Fuess, H. *Acta Crystallogr.* **2002**, *B58*, 463–470.
(47) Farrugia, L. J.; Frampton, C. S.; Howard, J. A. K.; Mallinson, P. R.; Peacock, R. D.; Smith, G. T.; Stewart, B. *Acta Crystallogr.* **2006**, *B62*, 236–244.
(48) Tsong-Song, H.; Yu, W. *J. Phys. Chem. A* **1998**, *102*, 3726–3731.
(49) Lee, C.-R.; Tan, L.-Y.; Wang, Y. *J. Phys. Chem. Solids* **2001**, *62*, 1613–1628.
(50) Chi-Rung, L.; Chih-Chieh, W.; Ko-Chun, C.; Gene-Hsiang, L.; Yu, W. *J. Phys. Chem. A* **1999**, *103*, 156–165.
(51) Abramov, Y. A.; Brammer, L.; Klooster, W. T.; Bullock, R. M. *Inorg. Chem.* **1998**, *37*, 6317–6328.
(52) Koritsanszky, T. S.; Coppens, P. *Chem. Rev.* **2001**, *101*, 1583–1627.
(53) Farrugia, L. J.; Evans, C. *J. Phys. Chem. A* **2005**, *109*, 8834–8848.
(54) Bader, R. F. W.; Matta, C. F. *Organometallics* **2004**, *23*, 6253–6263.

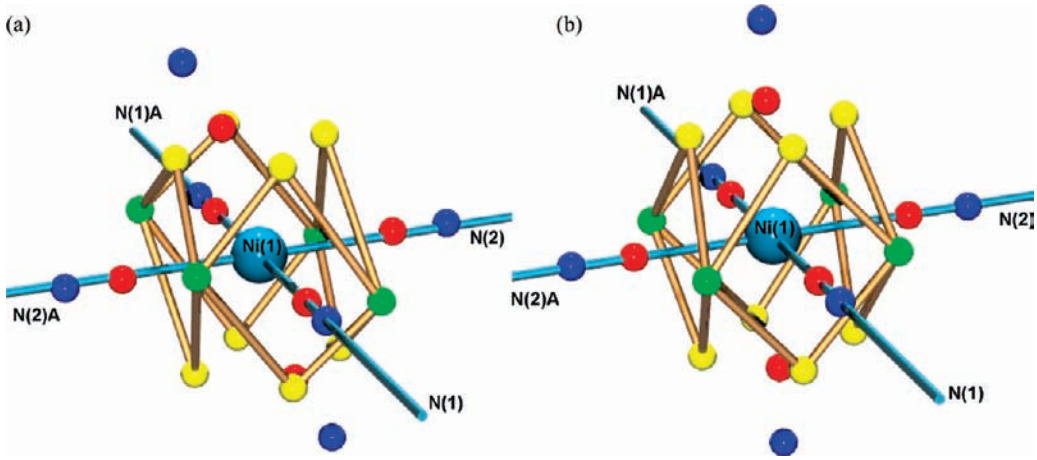

Figure 4. Atomic graphs of the Ni atom with multipole populations restricted (a) to C_i symmetry (model II) and (b) and D_{4h} symmetry (model IV) showing the critical points in $L(\mathbf{r})$. Color coding: (+3,−3) green, (+3,−1) yellow, (+3,+1) red, and (+3,+3) blue. The letter "A" denotes the $1 - X$, $1 - Y$, $1 - Z$ operation of symmetry.

Table 3. Average Values of Critical Points in the Negative Laplacian of $\rho(\mathbf{r})$ in the VSCC of the Ni Atom

model	CP type	$\rho(\mathbf{r}_{CP})$ [e Å^{-3}]	$L(\mathbf{r})$ [e Å^{-5}]	distance $\mathbf{r}$ [Å]
II	(+3,−3)	38.542	2135.484	0.290
	(+3,−1)	35.109	1242.088	0.296
	(+3,+1), *xyz*	28.994	129.531	0.304
		33.967	960.726	0.298
	(+3,+3), *xyz*	11.863	−539.205	0.426
		10.711	−297.645	0.468
IV	(+3,−3)	37.416	1952.201	0.291
	(+3,−1)	35.973	1335.025	0.295
	(+3,+1), *xyz*	28.583	93.393	0.304
		35.746	1191.134	0.296
	(+3,+3), *xyz*	11.882	−555.268	0.424
		10.300	−290.223	0.478

graph [8,12,6] of cuboid form close to the *XY* plane in the corners of the square, we can reproduce the [4,8,6] graph. Figure 4 presents atomic graphs of the Ni atom in the molecule **16Ni** with multipole populations restricted to C_i ($\bar{1}$) [model II] and D_{4h} (4/mmm) symmetry [model IV] of the central atom. Both graphs are similar, and the reduction of symmetry to C_i results in only minor changes in the CPs' locations. For example, for the D_{4h} symmetry, the (+3,−3) CPs are located in the plane created by the Ni and N atoms, whereas for C_i they are located above and below the plane. The topology of both graphs is exactly the same. However, the values of $\rho(\mathbf{r})$ and $L(\mathbf{r})$ presented in Table 3 are slightly different. Especially, the laplacian of $\rho(\mathbf{r})$ is very sensitive to changes in the model. Also, the $\rho(\mathbf{r})$ and $L(\mathbf{r})$ values for axially (along the *Z* axis) and equatorially located (+3,+1) and (+3,+3) CPs are different. The $\rho(\mathbf{r})$ and $L(\mathbf{r})$ values presented here are consistent with those published in the articles regarding charge density experiments in similar complexes, although the values for the equatorially located (+3,+1) CPs seem to be underestimated.[47,53]

The topology of the laplacian of $\rho(\mathbf{r})$ was also examined along the Ni(1)−N(1) bond (see Figure 5). The shape of $L(\mathbf{r}) \equiv -\nabla^2\rho(\mathbf{r})$ along the M−N bond is characteristic for the metal complexes. The negative laplacian curve exhibits two extrema in the vicinity of the Ni atom. The first one is the (+3,+1) CP located at a distance of about 0.30 Å from the atom, whereas the second one is about 0.47 Å from the Ni center. This agrees with calculation of the positions and

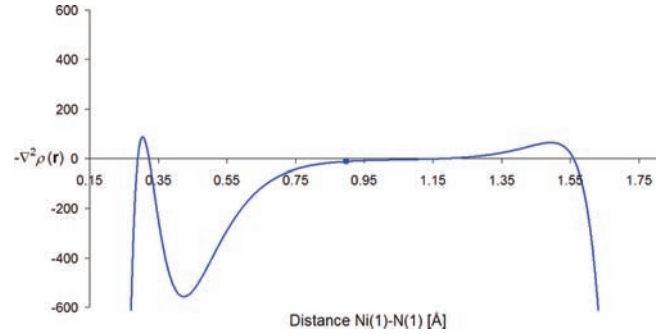

Figure 5. Negative laplacian of the electron density in [e Å^{-5}] along the Ni(1)−N(1) bond for model II. Bond critical point is marked by a bullet symbol.

values of these CPs presented above in Table 3. The curve predicts negative values at the BCP of the Ni(1)−N(1) bond located around 0.89−0.90 Å from the Ni nucleus. This is a typical situation of intermediate interactions occurring between the metal and ligands in the transition metal complexes. The $L(\mathbf{r})$ curve changes the sign after the BCP around 1.18 Å from the Ni and exhibits the third extremum—maximum—around 1.49 Å, corresponding to the bonding electron pair of the N1 atom.

The experimental and calculated—using the Gaussian 03 program[40]—electrostatic potential (ESP) surfaces for the **16Ni** molecule are presented in Figure 6. A positive isosurface surrounds the whole molecule. The experimental electrostatic potential exhibits very high positive values in the region of the propylene linker. The lowest, negative values of ESP are around the oxygen atoms (especially the carbonyl group) and Ni atom, despite the positive charge at the metal center. This can also be observed by calculation of the ESP property along the line perpendicular to the macrocyclic ring (see Figure 7).

The ESP changes sign at about 1.30 Å from the metal center and takes the lowest negative values (about −0.1e Å^{-1}) at about 1.88 Å from that center. Figure 7 shows also the curves of the $\rho(\mathbf{r})$ and $L(\mathbf{r})$ functions along the Ni(1)−X direction, where X stands for a point on the line perpendicular to the center of the Ni,N,N,N,N ring. The $\rho(\mathbf{r})$ function monotonously decreases to zero, whereas the $L(\mathbf{r})$ curve

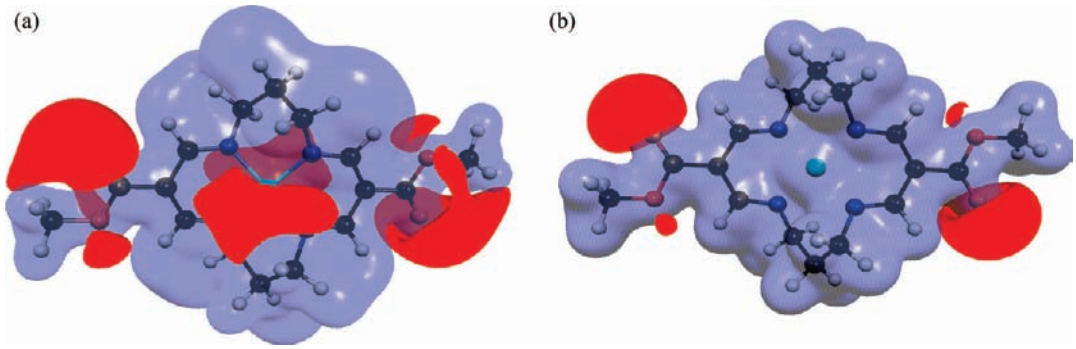

Figure 6. Isosurfaces of electrostatic potential for **16Ni**: (a) experimental − model II, (b) calculated. Blue and red surfaces correspond to +0.04 and −0.04*e* Å^{-1}, respectively.

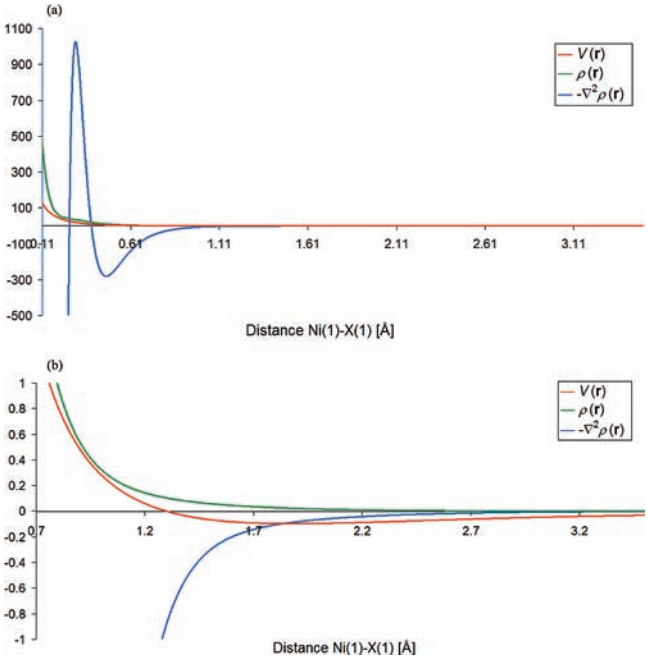

Figure 7. The electrostatic potential $V(\mathbf{r})$ [e Å^{-1}], $\rho(\mathbf{r})$ [e Å^{-3}], and $L(\mathbf{r})$ [e Å^{-5}] properties calculated for model II along the line Ni(1)−X perpendicular to the plane of the macrocyclic ring. The whole (a) and magnified regions (b) are shown. The numerical scale is common for all of the properties despite different units which are characteristic for a given particular property.

exhibits a maximum at about 0.30 Å and minimum at 0.47 Å from the metal center. These extrema can be easily identified as (+3,+1) and (+3,+3) CPs, respectively (see Table 3), and the whole shape of the curve is very similar to that of the Ni(1)−N(1) bond (see Figure 5). However, there is no BCP along the line in this case, since $\rho(\mathbf{r})$ is constantly decreasing. This is also indicated further by the shape of $L(\mathbf{r})$. After reaching the minimum, $L(\mathbf{r})$ converges to zero.

The calculated electrostatic potential for **16Ni** exhibits negative values in the same areas as the experimental one, except for the region around the Ni atom, where there is no negative value of ESP. The calculation was done for the free molecule without the crystal environment; therefore, the differences between those experimental and calculated isosurfaces are due to the interactions with the neighboring molecules in the crystal structure located above and below the plane of the macrocyclic ring. The shortest contact between the Ni and the H(8C) atom of the methyl fragment of the neighboring molecule (see Figure 8) is equal to 2.92 Å.

The 3d-Orbital Populations. The d-electron density can be described in terms of multipole density functions; therefore, it is possible to obtain d-orbital populations from the values of multipoles.[36,55−57] The comparison of the d-orbital populations for the Ni atom obtained from the refinement with local symmetry corresponding to the C_i and D_{4h} point groups is presented in Table 4. Only the models with an atomic scattering factor for the Ni center are listed (models II and IV). The corresponding values of the multipole populations are gathered in Table 6S (Supporting Information). The values of multipole and d-orbital populations for the Ni atom are very similar for models II and IV. The values of the multipoles allowed in the D_{4h} point group are at least 2 times higher than the other values of the multipoles (see models II and IV). Comparing those values, one can clearly see that the **16Ni** molecule is almost a square-planar complex. This is also supported by a low value of the sum of the squares of cross terms for d orbitals (see Table 4).

The experimental and theoretical d-orbital occupation orders for the Ni are quite similar, with the lowest population of the $d_{x^2-y^2}$ orbital. The values of the d-orbital populations roughly agree with the occupation order of the d-electron levels for the square-planar complexes derived from crystal field theory. However, the computed values are usually higher than the experimental ones. The average difference is in a range from 0.05 to 0.10*e*/orbital. The most different is the occupation of the d_{z^2} orbital. The total d-population is about 8.17 and 8.18 and about 8.37 and 8.74 for the experimental and theoretical data, respectively. The calculated NPA electronic configuration has a population of the 4s orbital equal to about 0.4. This is quite opposite to the experimental model, where the 4s population was set to be equal to 2, because of problems with the refinement of the 4s population (see Multipole Refinement for details).

Atomic Charges. The direct comparison of the atomic charges calculated by different methods can be cumbersome, since every method of electron partitioning is arbitrary. The

(55) Holladay, A.; Leung, P.; Coppens, P. *Acta Crystallogr.* **1983**, *A39*, 377–387.
(56) Stevens, E. D.; Coppens, P. *Acta Crystallogr.* **1979**, *A35*, 535–539.
(57) Sabino, J. R.; Coppens, P. *Acta Crystallogr.* **2003**, *A59*, 127–131.

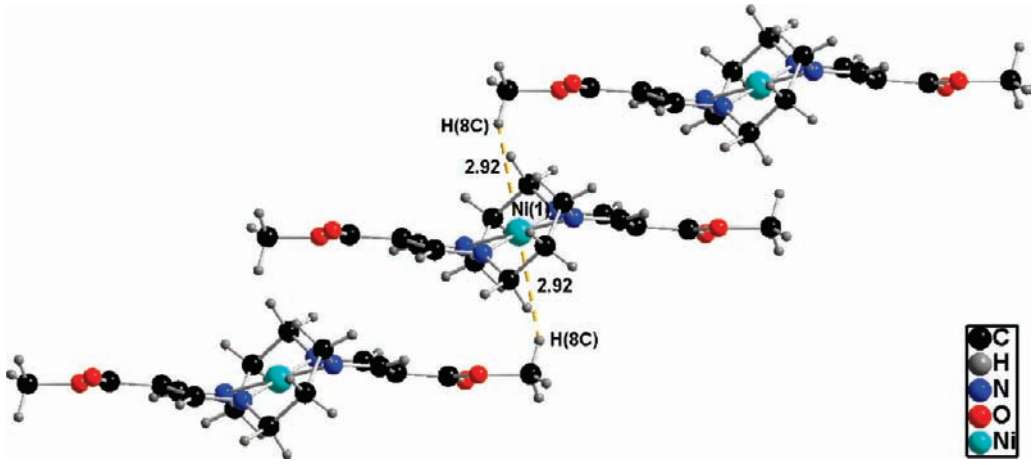

Figure 8. The crystal packing in the structure of **16Ni**. Short contacts between the Ni atoms and terminal groups of the neighboring molecules are presented.

Table 4. Experimental and Theoretical d-Orbital Populations Obtained for Ni Center for **16Ni**

16Ni	model II	model IV	DFT/B3LYP 6-31G* NPA	DFT/B3LYP LAN2DZ - Ni 6-31G** - other atoms NPA
symmetry	C_i	D_{4h}	C_i	C_i
d-orbital type	population	population	population	population
$d(z^2)$	1.79(1)	1.77(1)	1.843	1.946
$d(xz)$	1.89(1)	1.882(7)	1.938	1.974
$d(yz)$	1.86(1)	1.882(7)	1.942	1.977
$d(x^2-y^2)$	0.75(1)	0.71(1)	0.694	0.881
$d(xy)$	1.89(1)	1.93(1)	1.957	1.987
total d-pop	8.18	8.17	8.37	8.76
electronic configuration	$[core]4s^2 3d^{8.18}$	$[core]4s^2 3d^{8.17}$	$[core]4s^{0.45} 3d^{8.37}$	$[core]4s^{0.35} 3d^{8.76}$
cross terms[a]	population	population		
$d(z^2/xz)$	0.21(1)	0		
$d(z^2/yz)$	−0.03(1)	0		
$d(z^2/x^2-y^2)$	−0.12(1)	0		
$d(z^2/xy)$	−0.09(2)	0		
$d(xz/yz)$	0.03(2)	0		
$d(xz/x^2-y^2)$	0.14(1)	0		
$d(xz/xy)$	−0.17(1)	0		
$d(yz/x^2-y^2)$	0.02(1)	0		
$d(yz/xy)$	−0.004(14)	0		
$d(x^2-y^2/xy)$	0.06(1)	0		
$\sum (d_i/d_j)^2$	0.12	0		

[a] $\sum (d_i/d_j)^2$ is the sum of the squares of cross terms.

charges obtained from calculations with different basis sets (Mulliken and NPA) and from experimental data (monopole and AIM) are presented in Table 5. More detailed information about the AIM charges is presented in Table 7S—see the Supporting Information. According to AIM theory, each atom belonging to a molecule makes a uniquely defined contribution to the total electron density of the molecule. The volume of each atomic contribution, called the *atomic basin*, is a region in space where the paths of the gradient vectors of the electron density which originate at the infinity terminate at a given nucleus. The shape of an atom in a molecule is uniquely defined by its boundaries with other atoms and is open at the exterior of the molecule. The gradient paths never cross the *boundaries* of *atomic basins*. The atom domains can be identified as a zero flux surfaces around each atom. Such a partition projected on the molecular plane—together with bond and ring critical points—is illustrated in Figure 9. The AIM integrated charges are, therefore, defined as the difference between the formal number of electrons of an atom and the integral over the electron density within the atomic basin:

$$q_\Omega = Z_\Omega - \int_\Omega \rho(\mathbf{r})\, d\tau$$

The shape of the gradient lines for the metal atom basin is comparable to the gradient plots obtained for some similar complexes.[48,58]

The values of integrated atomic charges obtained for two different models (I and II) are presented in Figure 10. The **16Ni** molecule is neutral; therefore, the overall charge should be equal to zero. The summation of charges gives a value close to zero for all used models within an acceptable margin of error (second decimal place). Also, the errors of the integrals L_Ω for each atom are about 10^{-3} au. This gives certainty that the atomic basins were integrated properly. The

(58) Lee, J.-J.; Lee, G. H.; Wang, Y. *Chem.—Eur. J.* **2002**, *8*, 1821–1832.
(59) Jelsch, C.; Guillot, B.; Lagoutte, A.; Lecomte, C. *J. Appl. Crystallogr.* **2005**, *38*, 38–54.

Table 5. Atomic Charges for **16Ni**

16Ni	DFT/B3LYP LAN2DZ, Ni; 6-31G**, other atoms Mulliken population	DFT/B3LYP LAN2DZ, Ni; 6-31G**, other atoms natural population charges	AIM charges, model II
atom label	*q* [e]	*q* [e]	*q* [e]
Ni(1)	0.511	0.865	0.699
O(1)	−0.530	−0.636	−0.952
O(2)	−0.502	−0.565	−0.989
N(1)	−0.519	−0.572	−0.901
N(2)	−0.515	−0.573	−0.895
C(1)	−0.030	−0.271	0.283
C(2)	0.164	0.127	0.414
C(3)	−0.097	−0.345	−0.064
C(4)	0.157	0.120	0.619
C(5)	−0.030	−0.272	0.267
C(6)	−0.204	−0.485	0.108
C(7)	0.602	0.800	1.240
C(8)	−0.074	−0.330	0.526
H(2)	0.134	0.235	0.103
H(4)	0.126	0.229	0.030
H(1A)	0.135	0.247	−0.022
H(1B)	0.107	0.234	−0.007
H(5A)	0.137	0.248	0.055
H(5B)	0.103	0.232	0.073
H(6A)	0.109	0.242	−0.027
H(6B)	0.111	0.244	−0.020
H(8A)	0.110	0.220	−0.041
H(8B)	0.127	0.221	0.018
H(8C)	0.124	0.219	−0.147
sum	0	0	0.021

Ni atom in **16Ni** is predicted to be positive by all methods, except the monopole, and its charge is equal to 0.5−1.1*e* (only the values obtained from the DFT method are presented since the HF method usually gives too large values). The calculated Ni charge, especially by the DFT method with the LAN2DZ basis, is quite comparable to the experimental values of the AIM charges for models with the Ni-atomic scattering factor (0.5−0.7*e*). The O and N atoms are predicted to be negative by all methods. The lowest values of charge (−0.9 to −1.0*e*) for the nitrogen and oxygen atoms are obtained by the AIM model. Most of the carbon and hydrogen atoms carry a small positive charge. Surprisingly, the C(7) atom bonded to both oxygens has a very large positive charge. The value calculated by the AIM method seems to be too large (about 1.20*e*). However, the charge obtained by theoretical calculations is also rather high (about 0.6−0.8*e*). Contrarily, all methods predict a negative charge for the C(3) atom substituted by the methoxycarbonyl group.

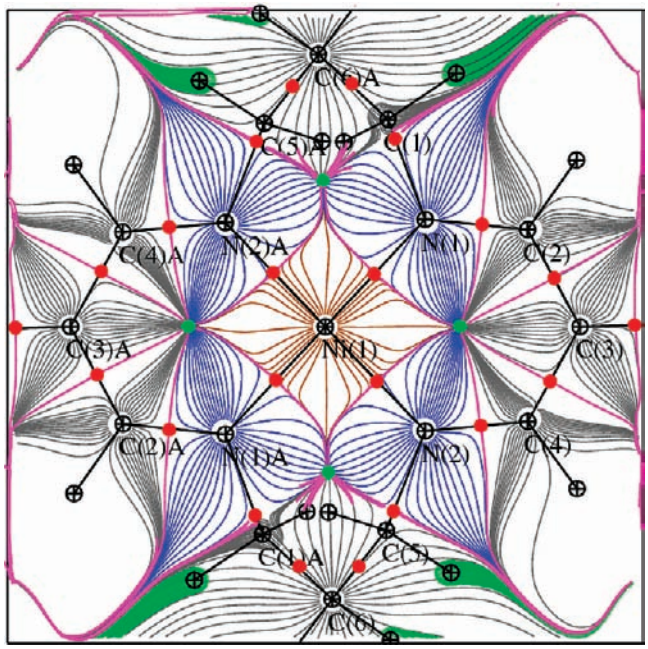

Figure 9. Gradient lines of the electron density calculated for model II, projected on the plane of the macrocyclic ring of **16Ni** obtained with the MoPro package.[59] The gradient lines in each atomic basin are colored according to chemical elements with the following assignment: Ni, brown; N, blue; C, gray; and H, green. The atomic basins are separated by the violet lines. Bright red and green dots denote positions of bond and ring critical points, respectively. The letter "A" in the atomic labels denotes the $1 - X$, $1 - Y$, $1 - Z$ operation of symmetry.

Upon comparing AIM charges for different models, several features are observed. More negative atomic charges are observed for all carbon atoms when the ionic scattering factor for the Ni atom is used. The charge of the metal ion is obviously much more positive for the formal occupation $4s^0 3d^8$ than for $4s^2 3d^n$. Generally, the greatest differences in the values of atomic charges between models I (III) and II (IV) are around the metal center. The obtained AIM charges (especially for the Ni center) are reasonable and close to those reported in the literature for similar systems when the atomic scattering factors were used for the metal center.[47,53]

Conclusions

Experimental and theoretical atomic charges and d-orbital populations were obtained for [3,11-bis(methoxycarbonyl)-1,5,9,13-tetraazacyclohexadeca-1,3,9,11-tetraenato(2-)-κ^4N]nickel(II) monocrystal (**16Ni**). Multipole refinement was accomplished using the Hansen and Coppens formalism. Several models were tested upon the following criteria: quality of the fit, convergence of the refinement, value of residual peaks and holes, and Hirshfeld's rigid-bond test. It turned out that the models with Ni-atomic scattering factors applied for the metal center are significantly better than those

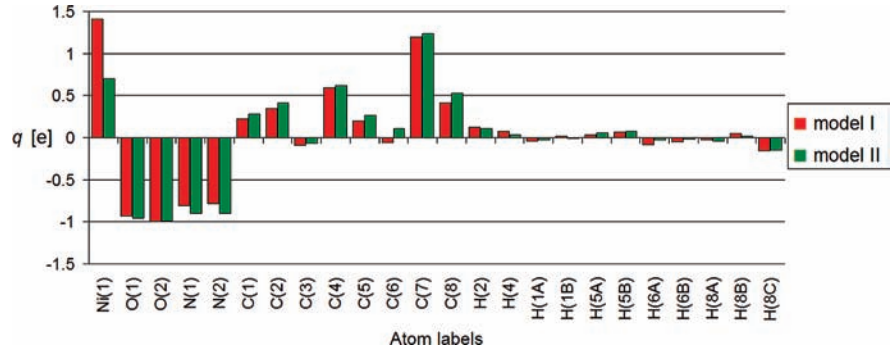

Figure 10. The values of the AIM atomic charges for **16Ni** obtained for models I and II.

with the Ni-ionic scattering factors. The properties of the final electron density distributions are very consistent and similar for all of the models tested. The d-orbital populations for Ni were calculated with C_i and D_{4h} symmetry restrictions on the multipoles to check symmetry degeneracy. The values of multipoles indicate an almost ideal square-planar symmetry for **16Ni**. The values of the d-orbital populations roughly agree with the occupation order of the d-electron levels for square-planar complexes derived from crystal field theory and are comparable with those obtained by the NPA method.

The continuous behavior of the negative laplacian [$L(\mathbf{r}) \equiv -\nabla^2\rho(\mathbf{r})$] was tested along selected Ni−N bond. The shape of this curve reflects the characteristic properties of the Ni−N bond with a positive value of the laplacian at the BCP. The laplacian in the plane of the macrocyclic ring shows four charge concentrations—$\underline{d}_{xy}$ orbitals—pointing toward the regions between the M−N bonds and charge depletions directed toward the (+3,−1) CPs of $L(\mathbf{r})$ for the nitrogen atoms. The atomic graphs of the Ni obtained, both for the C_i and D_{4h} symmetries, can be classified as the [4,8,6] form, still satisfying Euler's formula, which is consistent with the square-planar complex.

The theoretical atomic charges calculated for **16Ni** were compared to experimental ones calculated for four different models using the AIM method. The agreement is quite good when comparing the values for models with different symmetry restrictions and the same scattering factor for the Ni. All four models gave similar values of integration errors (lagrangian functions). The agreement between experimental AIM charges and calculated Mulliken or NPA charges is less satisfactory. However, some common trends are present. Both experimental and theoretical methods predict relatively high negative values of charges for the nitrogen and oxygen atoms and also a quite high positive charge for the C(7) atom. The DFT methods with the LAN2DZ basis and pseudopotential sets for the metal center give values of charge for the metal very close to those obtained by the experimental AIM method. Our results are consistent and comparable with those obtained for other square-planar and nonplanar Ni complexes already reported in the literature. Performed calculations of different properties indicate good reliability of the experimental charge density analysis for the **16Ni** compound.

Supporting Information Available: Figure 1S illustrating residual density map around the metal center, Tables 1S−7S containing numerical values of residual electron densities, values of statistical descriptors of the refinement, (*V*/*E*) ratio for the original and derived models, angular and radial integration grids for **16Ni** (AIM method), selected values of rho, laplacian and local kinetic and potential energy densities, multipole populations for different models applied, atomic charges as a function of the method applied, a brief chapter on additional multipoles applied and four CIF files. This material is available free of charge via the Internet at http://pubs.acs.org.

Acknowledgment. KW thanks the Ministry of Science and Higher Education - grant 1 T09A116 30 and the Foundation for the Polish Science - the Master (Mistrz) subsidy for financial support. BKD thanks for support through the grant number T204 074 32/20224 also from the Ministry of Science and Higher Education.

IC801835G